Supporting Information

Rapid Self-Healing in IR-Responsive Plasmonic Indium Tin Oxide/Polyketone Nanocomposites

Esteban Araya-Hermosilla[a], Alessio Gabbani[b], Arianna Mazzotta[a], Marina Ruggeri[b], Felipe Orozco[c], Valentina Cappello[a], Mauro Gemmi[a], Ranjita K Bose[c], Francesco Picchioni[c], Francesco Pineider[b], Virgilio Mattoli[a,*] and Andrea Pucci[b,*]

[a] Center for Materials Interfaces @SSSA, Istituto Italiano di Tecnologia, Viale Rinaldo Piaggio 34, Pontedera (PI) 56025, Pisa, Italy; esteban.araya@iit.it (E.A.-H.); virgilio.mattoli@iit.it (V.M.)
[b] Dipartimento di Chimica e Chimica Industriale, Università di Pisa, Via Moruzzi 13, 56124 Pisa, Italy;
[c] Department of Chemical Product Engineering, Engineering and Technology Institute Groningen (ENTEG), University of Groningen, Nijenborgh 4, 9747AG Groningen, The Netherlands; f.picchioni@rug.nl (F.P.)
* Correspondence: andrea.pucci@unipi.it (A.P.), Tel.: +39 0502219270 (A.P.); virgilio.mattoli@iit.it (V.M.), Tel.: + 39 050 883417

1. Polyketone characterization

We confirmed the functionalization of PK with FU by ATR-FT-IR and 1H-NMR spectroscopies Figure S1. Figure S1A shows the 1H-NMR spectra of PK after and before functionalization. The proton signal at 5.7 ppm (proton 1), which belongs to the pyrrole ring formed during the Paal-Knorr reaction, indicates the success of the functionalization process. The proton signals at 4.9 (proton 2), 5.9 (proton 4), 6.2 (proton 3), and 7.3 ppm (proton 5) confirmed the grafting of furan groups into the polymer. Figure S1B shows the ATR-FTIR spectrum of PK modified with FU. After functionalization, the intensity of the carbonyl group (1700 cm-1) decreases due to the disappearance of the 1,4-dicarbonyl moieties. The functionalized polyketone showed two peaks at 730 and 1010 cm-1 belonging to out-of-plane proton bending and C-O-C stretching of the furan pendant group, respectively. Also, at 3100 cm-1 appears the C=C-H stretching that belongs to the pyrrole ring. Overall, the decreased intensity of the carbonyl group and the peaks appearance at 730 and 1010 cm^{-1} confirm the polyketone modification. In the range of 1650-1500 cm^{-1}, weak peaks appear belonging to the C=N and C=C stretching in the pyrrole and furan ring. The asymmetrical and symmetrical stretching bands of aliphatic C-H of PK appear between 2969 and 2873 cm^{-1}.

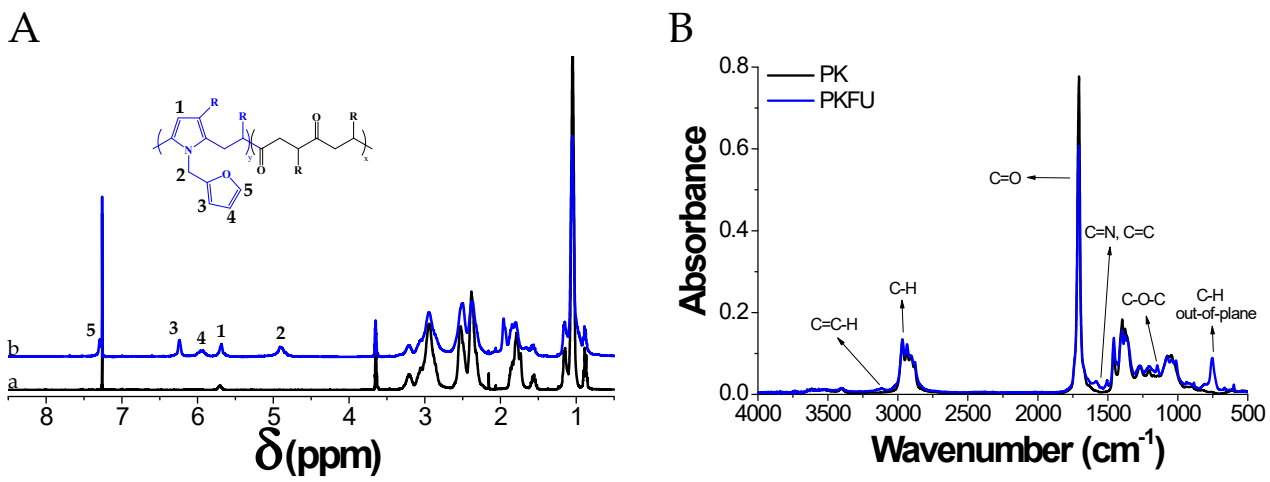

Figure S1. A) ^{1}H-NMR and B) ATR-FT-IR spectrum of PK before (black line) and after (blue line) the functionalization with FU.

2. Structural characterization of ITO NPs

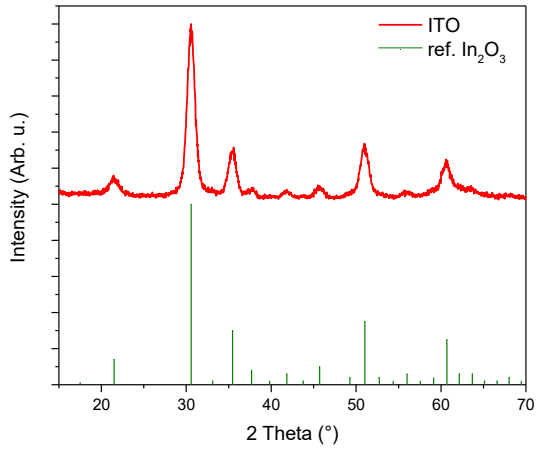

Figure S2. X-Ray Diffraction pattern of 7.5% Sn-In_2O_3 NCs, compared to the reference pattern of In_2O_3 (Powder Diffraction File PDF 06-0416).

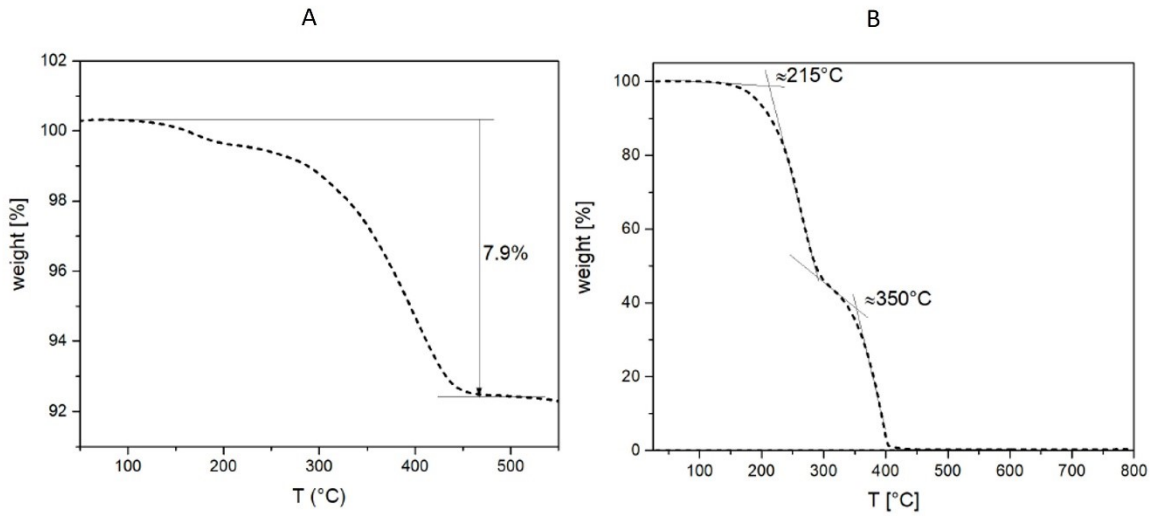

Figure S3. Thermogravimetric analysis of ITO NPs (A), and a 1:1 mixture of the surfactants (oleic acid and oleyl amine) used in the synthesis (B).

Table S1. Structural parameter of the NCs synthesized in this work.

	Initial Sn% [a]	Sn% (ICP-AES) [b]	D_{TEM} (nm) [c]	D_{XRD} (nm) [d]	a (Å) [e]	% wt. organic
ITO	7.5 %	7.2%	10.1 ± 2.0	9.31(4)	10.1372(3)	7.9

a) initial Sn % content in the reaction mixture; b) final Sn % content determined through ICP-AES; c) NCs average diameter obtained through statistical analysis of TEM images; d,e) mean crystal size and lattice constant obtained through XRD analysis. The errors of data obtained from XRD analysis are reported in brackets. f) organic fraction, determined through TGA analysis.

3. Optical properties of ITO NPs nanocomposites

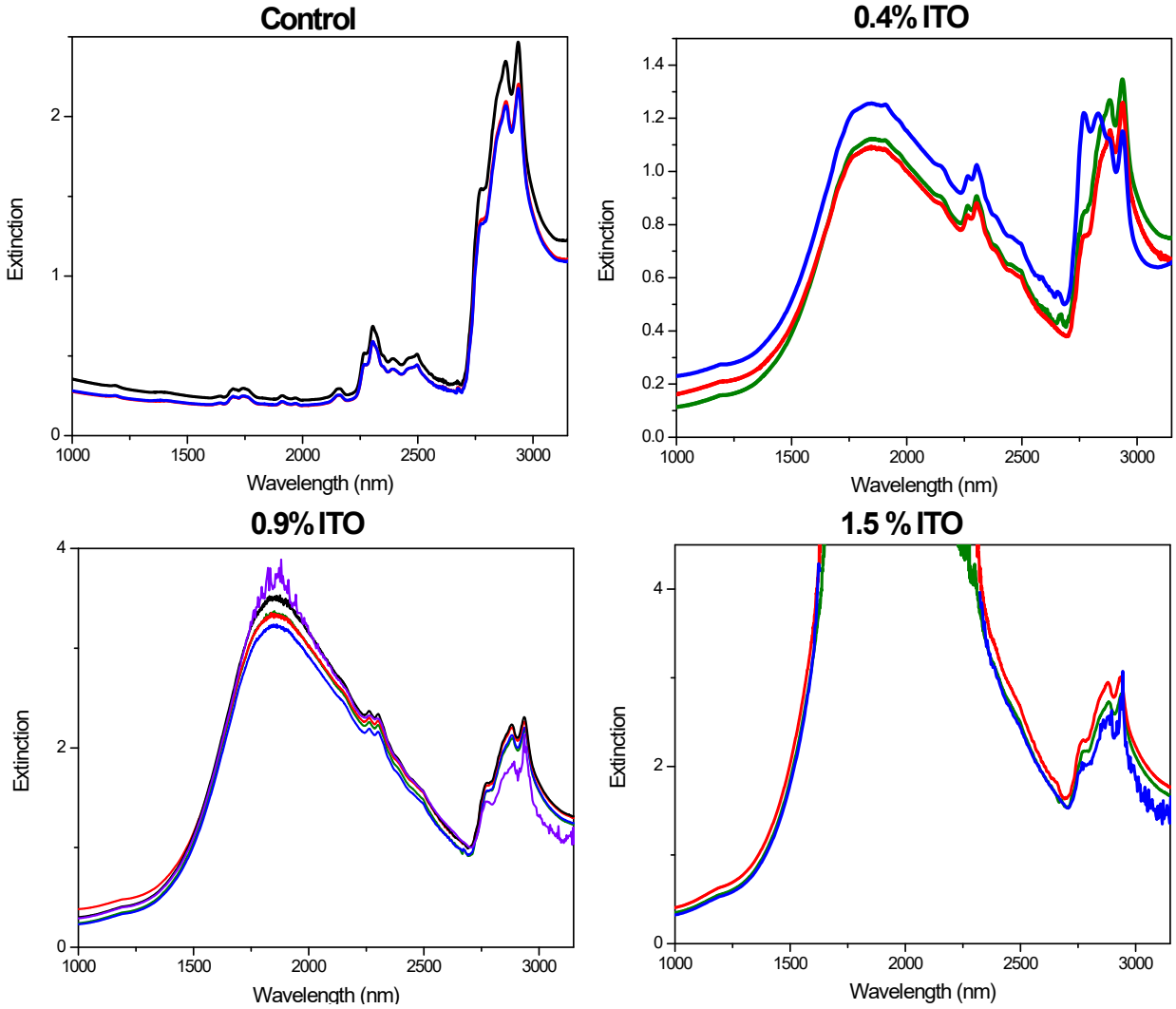

Figure S4. Extinction spectra of the nanocomposites collected on different portions of the samples (the investigated area have a diameter of 4 mm).

4. Modelling the optical response of ITO NPs

Since the ITO nanocrystals (NCs) are much smaller than incoming wavelength, their optical response can be modelled using Mie theory in the quasi-static approximation. The dipolar polarizability can be expressed as:[1]

$$\alpha(E) = \frac{\pi D^3}{2} \frac{\varepsilon_{NC}(E) - \varepsilon_m}{\varepsilon_{NC}(E) + 2\varepsilon_m},$$

Equation S1

where *D* is the NC diameter ε_{NC} is the dielectric function of the nanocrystal (NC) and ε_m the one of the solvent.

According to previous work on ITO NCs, we model the NC as a core@shell system, with a plasmonic active core and a depleted shell, where the electron density is negligible due to surface defects which reduce the volume accessible to conduction band electrons.[2,3] We thus express the core dielectric function (ε_C) according to Drude model:[4–6]

$$\varepsilon_C(E) = \varepsilon_\infty - i\frac{E_p^2\,\gamma - iE}{E\,E^2+\gamma^2}, \quad \text{with} \quad E_p^2 = \frac{\hbar^2 e^2 N}{m^* \varepsilon_0}$$

Equation S2

where E_p is the bulk plasma energy, N and m are the free electron density and effective mass, and γ is the damping parameter, ε_∞ is the background dielectric function ($\varepsilon_\infty = 4$ for ITO[2,3]), $\hbar$ is the Plank's constant (in eV/s), e is the electron charge and ε_0 is the permittivity of vacuum.

An empirical function for the frequency dependent damping parameter is used according to previous studies in the literature, [4–6] where γ_L and γ_H are respectively the low frequency and high frequency damping constant:

$$\gamma(\omega) = \gamma_L - \frac{\gamma_L - \gamma_H}{\pi}\left[tan^{-1}\left(\frac{\omega-\omega_x}{\omega_w}\right)+\frac{\pi}{2}\right],$$

Equation S3

The shell dielectric function (ε_S) was modelled as a pure dielectric material (with E_p=0). ε_S was thus set to the background polarizability of ITO, $\varepsilon_\infty = 4$.

The full dielectric function of the core@shell NC was then calculated according to Maxwell-Garnet equation:[7]

$$\varepsilon_{NC}(E) = \varepsilon_S\frac{(\varepsilon_C(E)+2\varepsilon_S)+2F(\varepsilon_C(E)-\varepsilon_S)}{(\varepsilon_C(E)+2\varepsilon_S)-F(\varepsilon_C(E)-\varepsilon_S)}$$

Equation S4

where F is the volume fraction of the active core, ε_C and ε_S dielectric function of the core and the shell respectively.

Equation S4 is then inserted in equation S1.

The NC absorption cross section σ can be expressed as:

$$\sigma = kIm[\alpha] = \frac{E\sqrt{\varepsilon_m}}{hc}Im[\alpha],$$

Equation S4

where E is the photon energy, h is the Plank constant and c the speed of light.

From the absorption cross section, the absorbance of the solution can be readily obtained using this equation:[5]

$$A = \frac{\#L\sigma}{\ln(10)} = \frac{3f_v L\sigma}{\ln(10)4\pi R^3}$$

Equation S5

where # is the particle number density, f_v is the volume fraction of the NCs in the medium, L is the optical path (the cuvette length in the case of a solution or the film thickness in the case of NPs embedded in a polymer matrix), R is the NCs radius.

The use of the described model to fit the optical spectrum is valid only for very small volume fractions (below 0.01).[5] The model is thus suitable for diluted solutions, such as ITO NCs dispersed in C_2Cl_4, or for polymer nanocomposites where the volume fraction of NCs is low. Moreover, the model does not consider inter-particle interaction, and is thus suitable only when the NCs are homogeneously distributed in the matrix and are well-separated from each other. T

To fit the spectra of ITO NCs dispersed in solution and in the polymer matrix, we employed the approach described above (equations S1-S5), using the dielectric constant of the matrix (2.26 for C_2Cl_4, and 2.24 for the polyketone matrix). The optical path of the cuvette (1 mm) was used for the solution while the film thickness (260 μm) was used for the nanocomposites. E_p, $\gamma(\omega)$, and the volume fraction of the active core *(F)* were left free during the fitting, such as the NCs volume fraction (f_v) in the medium. For the ITO dispersion, we use a solution with absorbance of 1. Applying equation S2 and using the plasma frequency E_p obtained from the fitting and $m^*=0.3m_e$ (taken from the literature[8,9]), we extract the free carrier concentration (8.3 10^{26} m^{-3}), which is reported in the main text. Fitting of the solution spectrum is reported in Figure S5.
Among the nanocomposites we did not perform the fit the one at higher ITO NPs content as the spectroscopic signal saturates at the plasmonic peaks. The fitting was performed in the range of the plasmonic resonance (1000-3000 nm) after subtracting the optical spectrum of the bare polymer from the one of the nanocomposite. The experimental spectra and fitting curves are then converted into transmittance values and plotted versus the photon wavelength in Figure 5 of the main text. The contribution of the polymer matrix was considered here as an additive term.

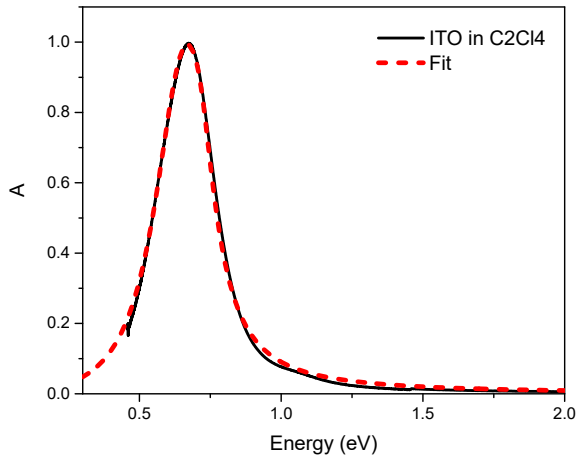

Figure S5. Fit of ITO NPs dispersed in C_2Cl_4.

Table S2. Parameters extracted from the fitting of the absorption spectra of the solution (in 1 mm cuvette) and the polymer films (260 μm thickness), using the fitting approach described above.

	Optical path[a]	Ep (eV)[b]	γ_L (eV) [b]	γ_H (eV) [b]	γ_x (eV) [b]	γ_w (eV) [b]	*F* [b]	f_v [b]	*wt %* [c]
Solution ITO in C_2Cl_4	1 mm	1.99	0.276	0.13	0.75	0.088	0.73	8.9×10^{-5}	0.035 %
Nanocomposites									

0.4% ITO	260 μm	1.99	0.276	0.130	0.75	0.041	0.73	4.4 x10^{-4}	0.30 %
0.9% ITO	260 μm	1.99	0.276	0.13	0.73	0.070	0.73	1.2 x10^{-3}	0.86 %

a) optical path is the one of the cuvette for the solution and the film thickness for the nanocomposite; b) parameters are left free during the fitting, and are defined as described above; F represent the fraction of active core; c) the NCs weight percentage is calculated from the volume fraction obtained in the fit using the density of ITO (7.140 g/cm^3), C2Cl4 (1.6 g/cm^3) and the polymer (around 1 g/cm^3)

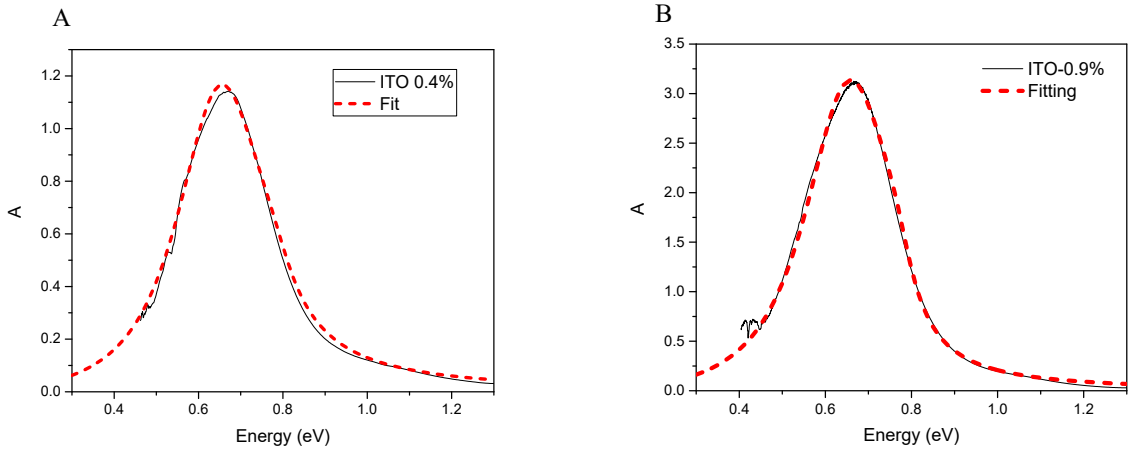

Figure S6. Fit of 0.4% (A) and 0.9% (B) polymer nanocomposites with the described optical model.

References

(1) Bohren, C. F.; Huffman, D. R. *Absorption and Scattering of Light by Small Particles*; Wiley: New York, 1983.

(2) Gibbs, S. L.; Staller, C. M.; Agrawal, A.; Johns, R. W.; Saez Cabezas, C. A.; Milliron, D. J. Intrinsic Optical and Electronic Properties from Quantitative Analysis of Plasmonic Semiconductor Nanocrystal Ensemble Optical Extinction. *J. Phys. Chem. C* **2020**. https://doi.org/10.1021/acs.jpcc.0c08195.

(3) Ghini, M.; Curreli, N.; Lodi, M. B.; Petrini, N.; Wang, M.; Prato, M.; Fanti, A.; Manna, L.; Kriegel, I. Control of Electronic Band Profiles through Depletion Layer Engineering in Core–Shell Nanocrystals. *Nat Commun* **2022**, *13* (1), 537. https://doi.org/10.1038/s41467-022-28140-y.

(4) Mendelsberg, R. J.; Garcia, G.; Milliron, D. J. Extracting Reliable Electronic Properties from Transmission Spectra of Indium Tin Oxide Thin Films and Nanocrystal Films by Careful Application of the Drude Theory. *Journal of Applied Physics* **2012**, *111* (6), 063515. https://doi.org/10.1063/1.3695996.

(5) Mendelsberg, R. J.; Garcia, G.; Li, H.; Manna, L.; Milliron, D. J. Understanding the Plasmon Resonance in Ensembles of Degenerately Doped Semiconductor Nanocrystals. *J. Phys. Chem. C* **2012**, *116* (22), 12226–12231. https://doi.org/10.1021/jp302732s.

(6) Hamberg, I.; Granqvist, C. G. Evaporated Sn-doped In2O3 Films: Basic Optical Properties and Applications to Energy-efficient Windows. *Journal of Applied Physics* **1986**, *60* (11), R123–R160. https://doi.org/10.1063/1.337534.

(7) Markel, V. A. Introduction to the Maxwell Garnett Approximation: Tutorial. *J. Opt. Soc. Am. A* **2016**, *33* (7), 1244. https://doi.org/10.1364/JOSAA.33.001244.

(8) Kimberly H. Hartstein; Schimpf, A. M.; Salvador, M.; Gamelin, D. R. Cyclotron Splittings in the Plasmon Resonances of Electronically Doped Semiconductor Nanocrystals Probed by Magnetic Circular Dichroism Spectroscopy. *J. Phys. Chem. Lett.* **2017**, *8* (8), 1831–1836. https://doi.org/10.1021/acs.jpclett.7b00494.

(9) Gabbani, A.; Sangregorio, C.; Tandon, B.; Nag, A.; Gurioli, M.; Pineider, F. Active Magnetoplasmonics with Transparent Conductive Oxide Nanocrystals. *arXiv:2104.07772 [cond-mat, physics:physics]* **2021**.

5. Details on the characterization of thermal behaviours and self-healing properties of the nanocomposite

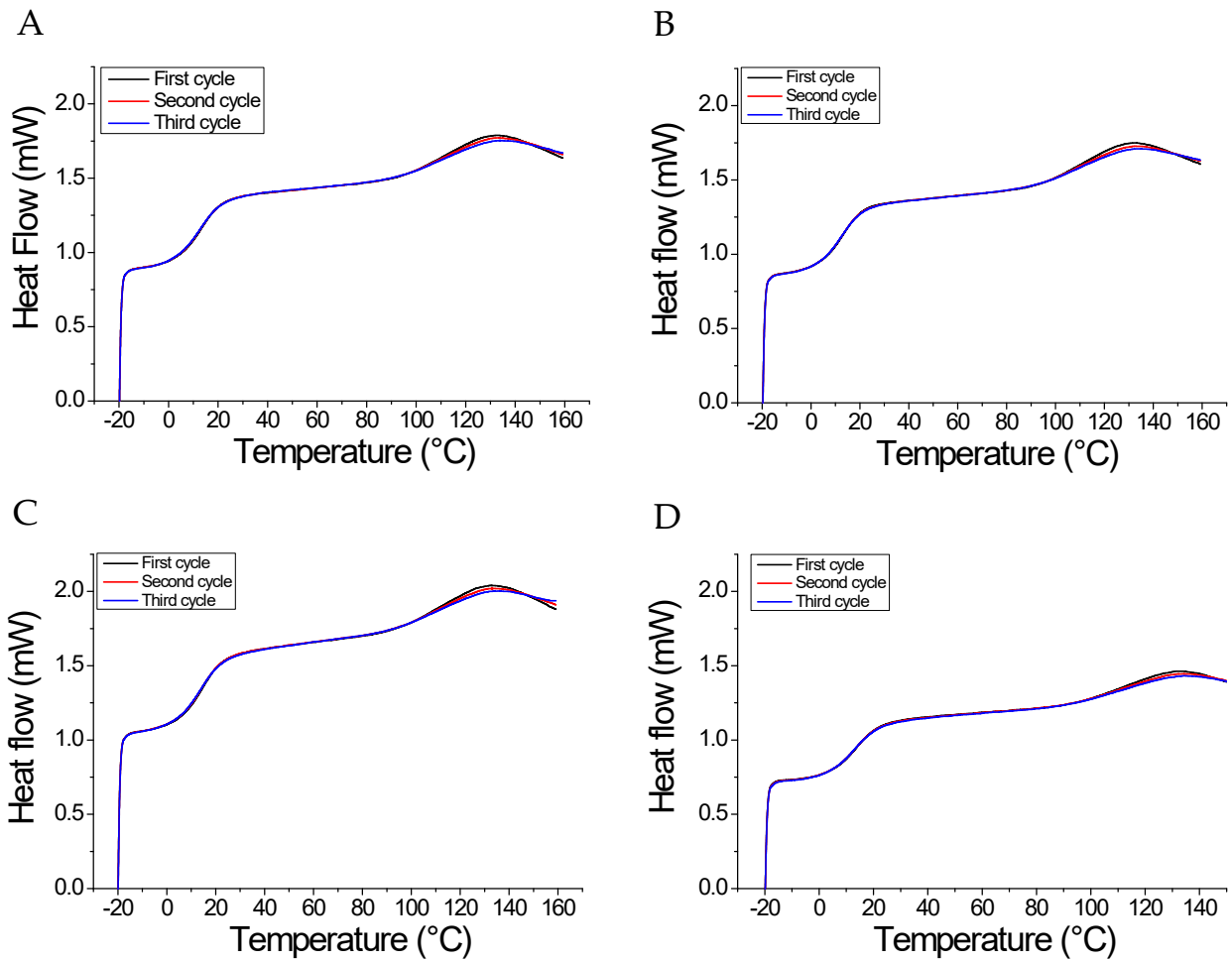

Figure S7. DSC cycles of the PK thermoset matrix (A) and the respective nanocomposites at a wt.% concentration of ITO NCs of 0.4 wt% (b) 0.9 wt% (C) and 1.5 wt% (D).

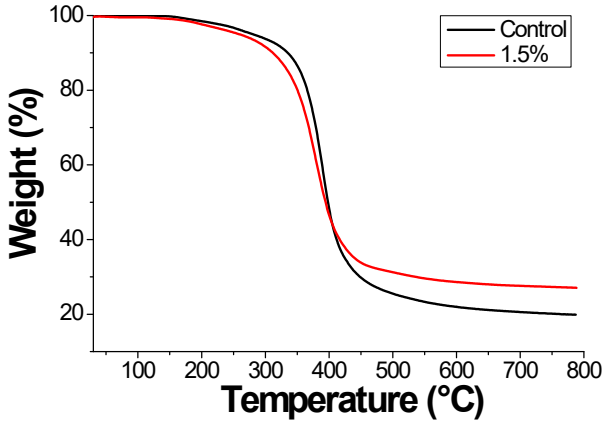

Figure S8. Thermogravimetric analysis of the polymeric matrix and the composite at the highest ITO NCs content.

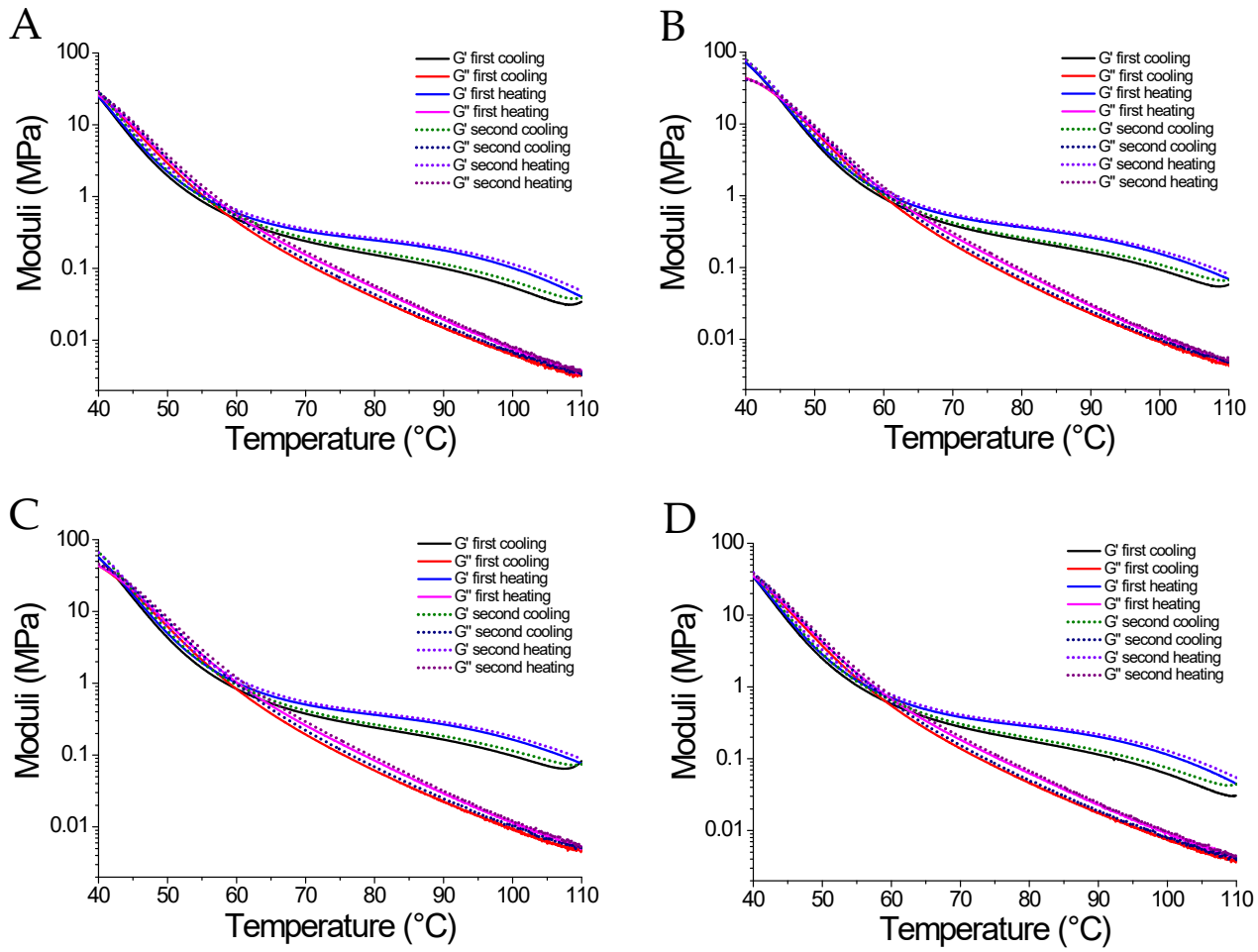

Figure S9. Thermomechanical properties (storage G' and loss G'' loss modulus) of the nanocomposites determined by rheology. A) control (bare thermoset matrix), B) 0.4 wt.%, C) 0.9 wt.%, D) 1.5 wt.% of the ITO NCs.

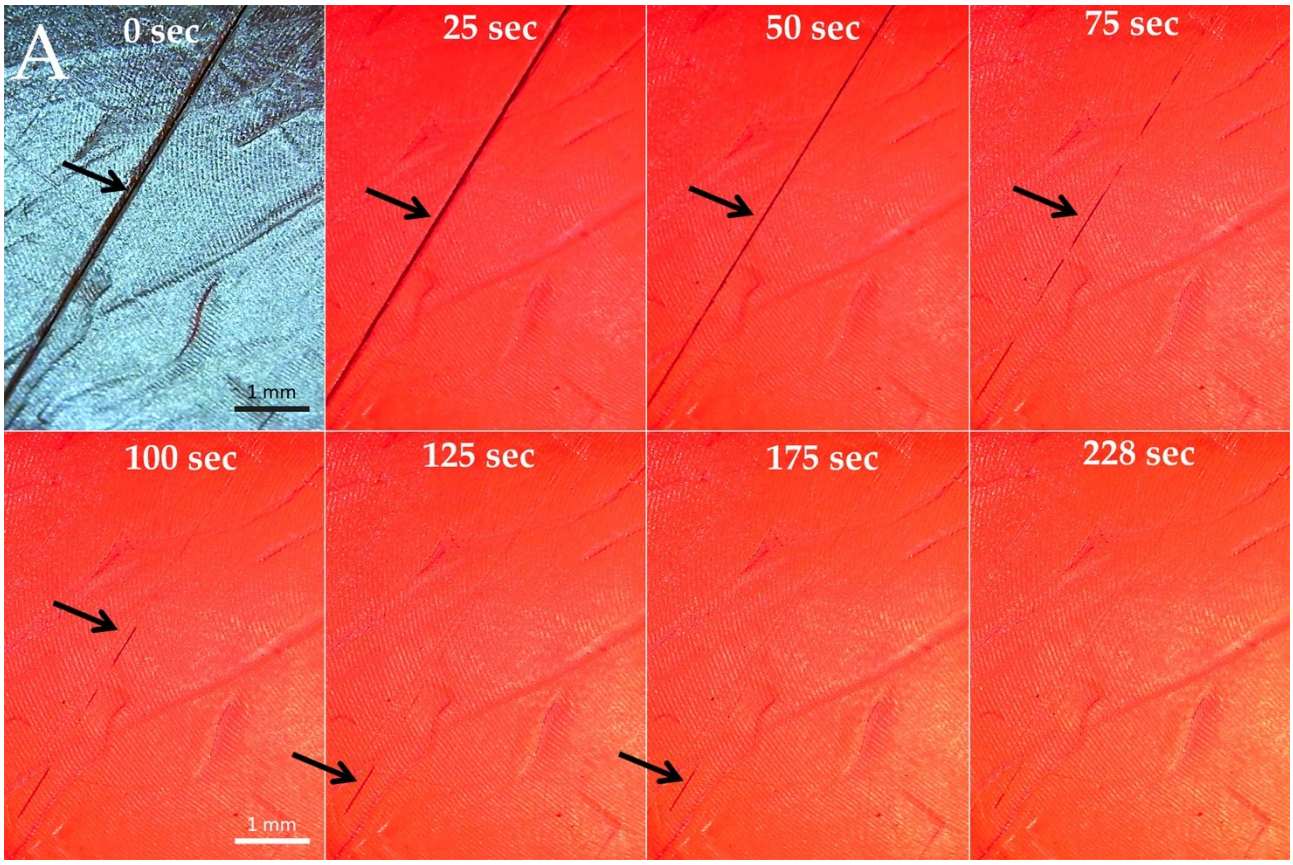

Figure S10. Microscope image of the control's self-healing process.

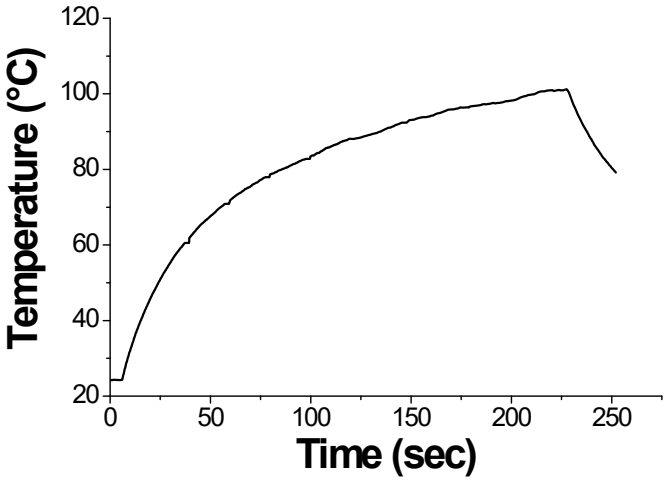

Figure S11. Surface temperature as a function of the IR illumination time of the control's self-healing process (Figure S9)

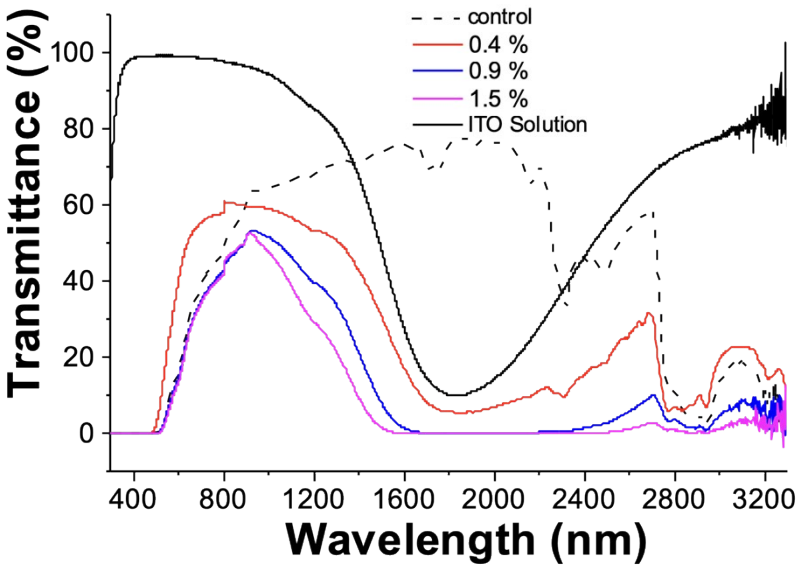

Figure S12. UV-VIS-NIR transmittance spectra of the nanocomposites and the ITO NCs solution

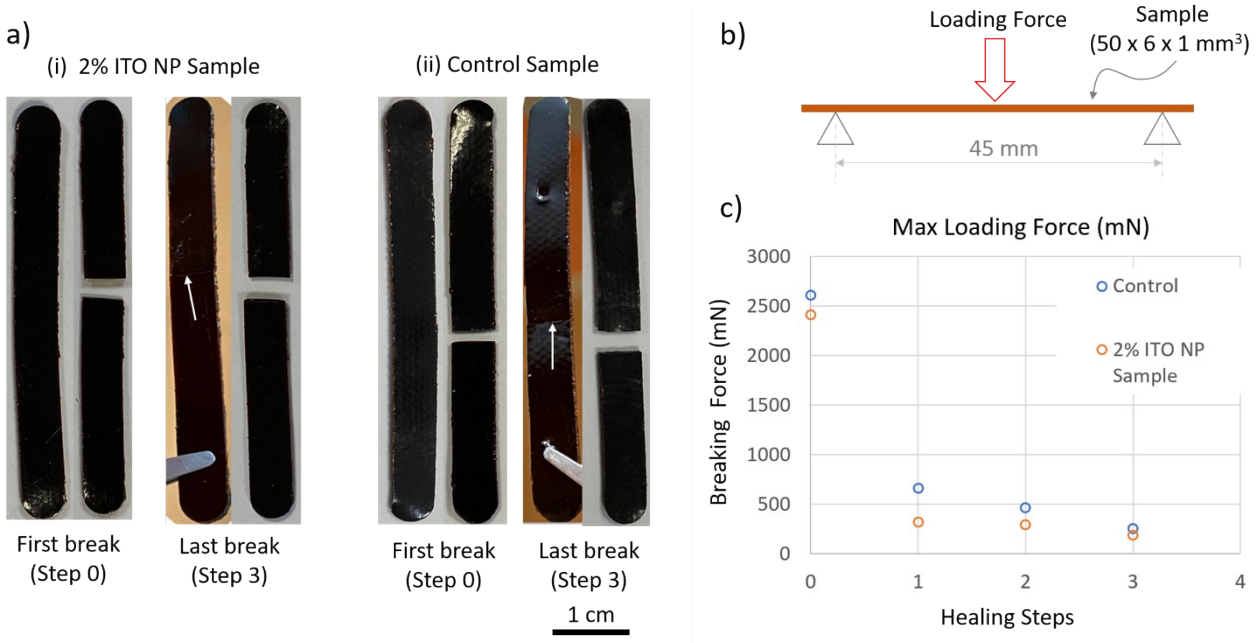

Figure S13. IR induced self-healing test by bulk fracture. The beam-shaped specimen containing 2% of ITO nanoparticles (a-i) and the control one (without ITO nanoparticles, b-ii) has been subjected to a controlled load (in simply supported, center load configuration, see (b)) to determine the breaking force before and after the healing treatment induced by a 300W IR lamp. The breaking and healing process has been repeated three times. The maximum loading measured is reported in (c). The healing process have been performed by adjusting the lamp distance from the sample to reach the target temperature of about 90°-95° on the sample (measured with a IR thermos-camera), and to keep it constant for 5 minutes. Test results show that ITO containing sample and control sample evidenced a similar mechanical behaviour, indicating that the presence of nanoparticles, while providing thermoplasmonic characteristics, does not influence substantially the mechanical properties of composite. In particular, in both cases the maximum load substantially decreases after

the first breaking event and at each subsequent test the specimen fracture appears located in the same position of the previous one. This is somehow expected for two reasons: firstly, the complete fracture could involve the interruption of the polymeric network not only at level of Diels-alder crosslinking and hydrogen bonds interactions, but probably also at level of polymeric chains; the latter cannot be re-established by heating. Additionally, a part of effect could be due to the not perfect matching of the fractured surfaces during the IR healing, that crates a weakness point in the structure.